Dynamic Modeling and Motion Control of a Soft Robotic Arm Segment

Zhi Qiao, Pham H. Nguyen, Panagiotis Polygerinos, and Wenlong Zhang*

***Abstract*— Soft robotics has shown great potential in manipulation and human-robot interaction due to its compliant nature. However, soft systems usually have a large degree of freedom and strong nonlinearities, which pose significant challenges for precise modeling and control. In this paper, a linear parameter-varying (LPV) model is developed to describe the dynamics of a soft robotic arm segment. Given the different actuation mechanisms, the LPV models for elongation and bending motions are identified through experimental data. A state-feedback H_∞ controller is designed for the LPV model using a linear matrix inequality (LMI). Simulation of the state-feedback controller indicates that the closed-loop system is stable but with steady-state errors. As a result, an iterative learning control (ILC) with P-type learning function is implemented to improve the tracking performance. Simulation results of the ILC+state-feedback controller show steady-state errors are significantly reduced with iterations. The ILC+state-feedback controller successfully moves the soft robotic arm segment to its desired position within several iterations in experiments.**

I. INTRODUCTION

The fast-growing interest in soft robotics comes from its various intrinsic properties, such as its safe interaction with the human body, high power-to-weight ratio, compliant to the environment it interacts with, and low-cost fabrication. Some examples are readily seen in the field of manipulation [1] and wearable systems [2]. The contribution to various soft actuators includes pneumatic artificial muscles [3], inflatable structures [4], fluidic-elastomeric actuators [5], and origami structures [6]. A topic of paramount importance is the modeling and control of such systems [7].

The goal of designing a control system for soft robots is to find a set of inputs based on feedback to reach its desired shape or position. If the transient state is not of interest, the model of an actuator can be estimated through measurements at the steady state. In [8], researchers used a constant curvature model to estimate the final posture of a multi-link soft arm. In [9], the authors presented an FEA method to generate control inputs based on the desired deformation. In [10], it was assumed that the expansion force in the actuator walls produced by air pressure was equivalent to the contraction force due to the material deformation and they built a pressure dependent curvature model to estimate the actuator conformation at the steady state. Since these models focus only on the steady-state performance and ignore the system dynamics, the corresponding controller cannot be used to achieve fast and dynamic tasks.

Dynamic models of the soft robotics are generally complicated, due to their nonlinear material properties and generally slow responses to the pressure stimuli. To capture the dynamic behaviors and the nonlinear properties of soft actuators, Cosserat rod and mass-damper-spring based models are proposed in [11], [12]. In [11], the authors provided a piecewise-constant curvature model to estimate the dynamics of an elastic tube robot. The computational cost of this model increased significantly with an increasing number of actuators. In [12], the author proposed a mass-damper-spring based model which was built through a network of mass-spring-damper links and their accuracy was improved with a higher number of the links. It was also found that the spring coefficient of the system was linearly dependent on its control input, i.e., air pressure, while the mass and damper coefficients were assumed to be constant values. The dynamics of this input dependent system can be described using a linear parameter-varying (LPV) model [13].

Besides modeling, soft robot control has received much attention recently. To drive the soft robots to their desired postures, sliding mode and model predictive controllers were designed to track the reference trajectory [14], [15]. However, it is very challenging to achieve fast-tracking and strong robustness simultaneously with feedback control only for complex soft robot models. To address this problem, an iterative learning controller (ILC) is proposed to improve the tracking performance by reducing the delay in the transient period and rejecting the unknown repetitive disturbances [16]. A combination of the feedback controller and an ILC could perform better than each method individually. The contributions of this paper are outlined as follows:

- An LPV model is developed and experimentally validated for an elastomer-based soft robotic arm segment.
- A robust H_∞ state-feedback controller and a combined controller with ILC for the LPV model are designed.
- A custom experimental platform and a segment of the soft robotic arm are used to validate the stability of the H_∞ control and the improved tracking through ILC.

The remainder of the paper is organized as follows: Section II discusses the soft arm design and the experimental platform setup. Section III introduces the LPV model for one soft segment and its parameter identification. Section IV discusses the state-feedback H_∞ controller and ILC design. Section V presents the simulation results of the closed-loop system with two controllers (state-feedback and

This work was supported in part by the National Science Foundation under Grant CMMI-1800940.

Z. Qiao is with School for Engineering of Matter, Transport, and Energy, Arizona State University, Tempe, AZ, 85287, USA. Email: Zhi.Qiao.1@asu.edu.

P. H. Nguyen, P. Polygerinos, and W. Zhang are with The Polytechnic School, Arizona State University, Mesa, AZ, 85212, USA. Email: nhpham2@asu.edu, polygerinos@asu.edu, Wenlong.Zhang@asu.edu.

*Address all correspondence to this author.

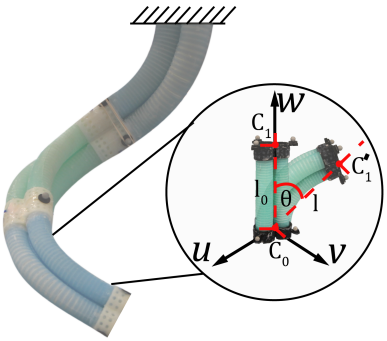

Fig. 1: The soft robotic arm with a zoom-in view of a single segment. $\boldsymbol{u}$, $\boldsymbol{v}$ and $\boldsymbol{w}$ are the orthogonal axes. C_0 and C_1 are the center points of the bottom and the top surface where C_0 is the origin of the coordinate. $\boldsymbol{l}_0$ and $\boldsymbol{l}$ are the vectors between the two center points at the initial time and any time instance where θ is the angle between $\boldsymbol{l}$ and $\boldsymbol{w}$.

ILC+state-feedback). Section VI presents the experimental results. Section VII concludes the paper and discusses future work.

II. HARDWARE DEVELOPMENT AND TESTING

The soft robotic arm is made of elastomeric material introduced in our previous work [17]. In this paper, we focus on the control of a single segment [18] of the soft robotic arm. The segment is manufactured by fusing three ring-reinforced tubular actuators (RRAs) in parallel to constrict the radial motion while promoting extension motion of the actuator using Acrylonitrile Butadiene Styrene (ABS) circular ring reinforcements in an equilateral triangular fashion. The material of the elastomeric actuator body has a shore hardness of 30A (Dragon Skin 30, Smooth-On Inc., PA). The segments are designed to be 160 mm long and have various degree of freedoms depending on the inflation combination of the three RRAs in each segment. The coordinate frame of the soft arm is shown in Fig. 1. The custom soft robotics evaluation platform is designed to sense, actuate, and record motion trajectories [17], shown in Fig. 2.

III. MODELING AND PARAMETER IDENTIFICATION

In this section, a mass-damper-spring model [19] is employed to describe the dynamics and the end-effector position of the soft arm. The model input is air pressure and outputs are the bending angle and distance between the center points of the bottom and top surfaces. It should be noted that only these two outputs are not enough to uniquely define the 3D position of the end-effector. In this paper, as a proof of concept, only one output will be controlled during the simulation and experiment. The more comprehensive full system model is left as future work. In elongation motion, all three chambers of the actuator will be inflated with the same pressure while in bending motion only one chamber will be activated. Therefore, the dynamic models for elongation motion and bending motion are identified individually.

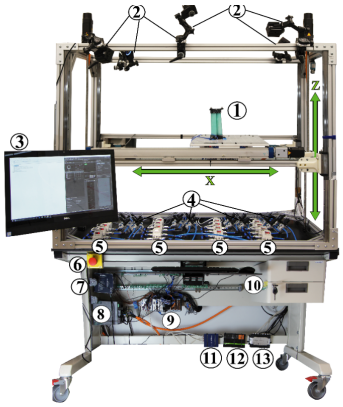

Fig. 2: Experimental platform to monitor and control the soft segment. (1) The 3-chambered segment. (2) Motion capture system. (3) Computer system. (4) Thirty-two high-switching valves. (5) Sixteen pressure regulators. (6) Emergency stop button. (7) Power supply. (8) Motor drivers. (9) NI compact-RIO (cRIO) controller. (10) Keyboard and mouse. (11) Ethernet adapter. (12) 8-port Gigabit PoE/PoE+ switch for use with Ethernet cameras. (13) eSync 2 box to synchronize motion capture readings with NI system.

A. LPV Model of the Soft Arm

In [19], each segment was considered as a rigid parallel mechanism which provides a more accurate description in elongation motion than in bending motion. In this paper, the end-effector position of the segment is described as the distance changes between the center points of the top and bottom surfaces L and angle changes θ between the initial posture and the posture at any time instance, as shown in Fig. 1. It should be noted that when only one chamber is actuated the bending axis of the segment is parallel with the line that goes through the centers of the other two chambers at the bottom surface. With the soft arm fixed on the platform, the direction of the rotation axis is constant in the global coordinate. With the knowledge of the rotation axis direction, the 3D position of the end-effector can be represented using L and θ, shown in Fig. 1.

The position and angle changes, $L(t)$ and $\theta(t)$, are calculated as follows.

$$L(t) = ||\boldsymbol{l}(t)|| - ||\boldsymbol{l}_0|| \tag{1}$$

$$\theta(t) = cos^{-1}\frac{\boldsymbol{l}(t)\cdot\boldsymbol{w}_0}{||\boldsymbol{l}(t)||} - cos^{-1}\frac{\boldsymbol{l}_0\cdot\boldsymbol{w}_0}{||\boldsymbol{l}_0||} \tag{2}$$

where $\boldsymbol{l}(t) = C_1(t) - C_0(t)$ is the end-effector position vector at any time instance. $\boldsymbol{l}_0 = \boldsymbol{l}(t=0)$ is the initial position vector of end-effector. $\boldsymbol{w}_0$ is a unit vector along $\boldsymbol{w}$ axis. In this paper, we assume that only one chamber will be inflated during the bending motion.

As mentioned in [15], the torque generated by a pneumatic actuator can be estimated as a linear function of the input pressure p such that the dynamic model of the soft arm segment is expressed as follows (the time index is omitted for brevity in the following sections)

$$M(p)\ddot{\boldsymbol{q}} + B(p)\dot{\boldsymbol{q}} + K(p)\boldsymbol{q} = f(p) \tag{3}$$

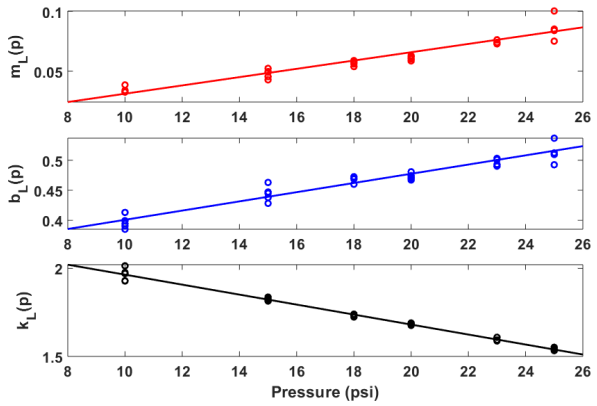

(a) Estimated system parameter for length

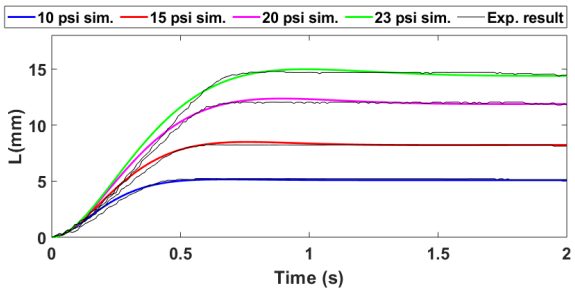

(b) Simulation vs. experimental results

Fig. 3: The system parameter estimation and simulation result for elongation motion

TABLE I: Parameter for elongation motion ($y = a_1 x + a_0$)

Variable	a_1	a_0	R^2
$m_L(p)$	$3.471E-03$	$-3.612E-03$	0.9027
$b_L(p)$	$7.657E-03$	$3.243E-01$	0.9245
$k_L(p)$	$-2.835E-02$	2.248	0.9892
$f(p)$	1	0	N/A

where $\boldsymbol{q} = [L, \theta]^T$ is the state vector of the system. Suggested by the collected experimental data whose input pressure ranges from 10 to 25 psi, a decoupled dynamic model is presented to bending motion dynamics. This will also be validated in experimental results later in Fig. 4(c) Therefore, $M(p), B(p)$ and $K(p)$ are diagonal matrices and only dependent on the input pressure. The simplified LPV model can be described by:

$$\begin{bmatrix} m_L(p) & 0 \\ 0 & m_\theta(p) \end{bmatrix} \ddot{\boldsymbol{q}} + \begin{bmatrix} b_L(p) & 0 \\ 0 & b_\theta(p) \end{bmatrix} \dot{\boldsymbol{q}} + \begin{bmatrix} k_L(p) & 0 \\ 0 & k_\theta(p) \end{bmatrix} \boldsymbol{q} = f(p) \tag{4}$$

B. Parameter Identification

For each type of motion, there are three parameter matrices that need to be identified, i.e., the equivalent mass, damping, and spring coefficient matrices. In elongation motion, a set of step input (fixed pressure) is given to all three chambers and only the length changes L are recorded. Using the pressure and length changes as the model input and output, the required parameters are calculated using the MATLAB System Identification Toolbox and presented in Fig. 3(a).

Using the linear least square method, the coefficients of the linear function are estimated and shown in Table I. It is observed that all three parameters are linearly dependent on the input pressure since the R^2 values are all close to one. The fitted linear functions are presented in Fig. 3(a).

Similarly, the system parameters for bending motion are identified through a set of experiments with fixed pressure inputs. Only one chamber is inflated during the test to simplify the modeling process. The experimental results with

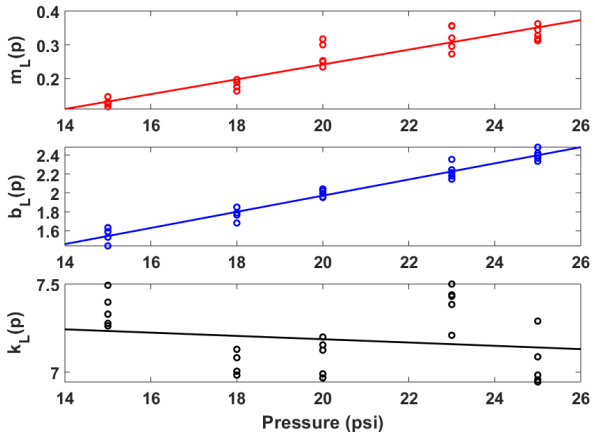

(a) Estimated system parameters for length

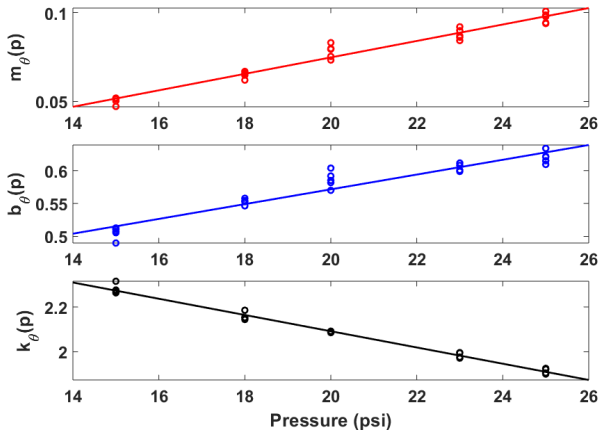

(b) Estimated system parameters for angle

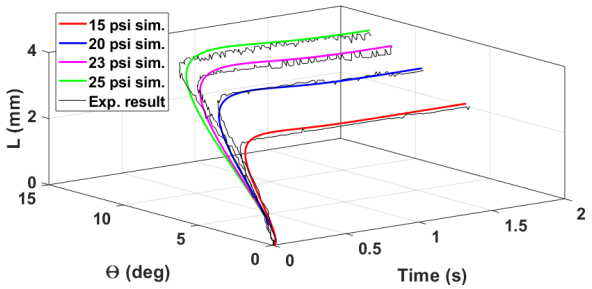

(c) Comparison between simulation and experimental results

Fig. 4: The system parameter estimation and simulation result for bending motion

TABLE II: Parameter for bending motion ($y = a_1 x + a_0$)

Variable	a_1	a_0	R^2
$m_L(p)$	$2.191E-02$	$-1.962E-01$	0.8699
$b_L(p)$	$8.517E-02$	$2.677E-01$	0.9553
$k_L(p)$	$-9.350E-03$	7.374	0.0334
$m_\theta(p)$	$4.624E-03$	$-1.768E-02$	0.9664
$b_\theta(p)$	$1.123E-02$	$3.469E-01$	0.9194
$k_\theta(p)$	$-3.622E-02$	2.816	0.9890
$f(p)$	1	0	N/A

their estimated linear functions are shown in Figs. 4(a) and 4(b) for the L term and θ term, respectively. The identified parameters in Table II demonstrate that all model parameters except k_L are linearly dependent on the input pressure.

Comparing the experimental data presented in Figs. 3(b) and 4(c), it is found that the distance changes at the steady state are relatively small in bending motion than elongation which indicates that the $k_L(p)$ term is independent of the pressure and can be treated as a constant (this is also the reason why the R^2 for $k_L(p)$ is so small). It is also noticeable that given the same step input (fixed pressure), the LPV model simulations are able to match the corresponding experimental results. This indicates that the LPV model well captures the dynamics of the soft arm and supports the decoupled system assumption mentioned above.

IV. MOTION CONTROL OF THE SOFT ARM SEGMENT

A. Motion Control with a State-feedback Controller

This subsection focuses on robust motion control of the soft arm motion. Take the elongation motion as an example, it can be rewritten as the following second-order system

$$\dot{x} = A(p) \cdot x + B(p) \cdot (p + d), \tag{5}$$

$$y = C \cdot x, \tag{6}$$

where $x = [L \quad \dot{L}]^T$ is the system state vector, p represents the pressure input, and d is the external disturbance from the valve and pressure regulator. The system matrices for elongation motion are shown as follows:

$$A(p) = \begin{bmatrix} 0 & 1 \\ -\frac{k_L(p)}{m_L(p)} & -\frac{b_L(p)}{m_L(p)} \end{bmatrix}, B(p) = \begin{bmatrix} 0 \\ \frac{1}{m_L(p)} \end{bmatrix}, C = \begin{bmatrix} 1 \\ 0 \end{bmatrix}^T$$

In this paper, we propose to use a fixed-gain state-feedback controller $u^{fb} = K \cdot x$ and the resulting closed-loop dynamics is

$$\begin{bmatrix} \dot{x}_{cl} \\ y \end{bmatrix} = \begin{bmatrix} A(p) + B(p) \cdot K & B(p) \\ C & 0 \end{bmatrix} \begin{bmatrix} x_{cl} \\ d \end{bmatrix}. \tag{7}$$

where $x_{cl} \in \mathbb{R}^2$ is the closed-loop system state.

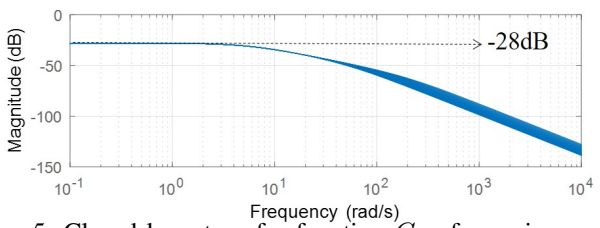

Fig. 5: Closed-loop transfer function G_{yd} for various pressure inputs in Φ_p

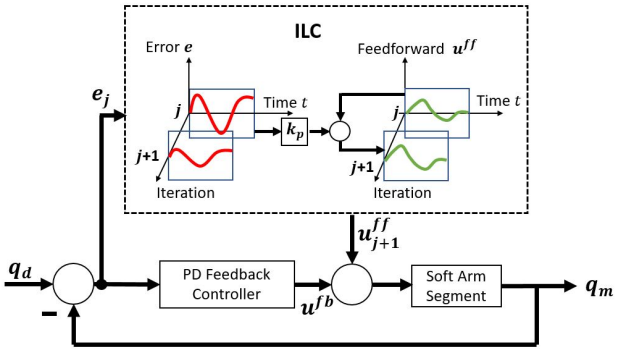

Fig. 6: Block diagram for ILC+state-feedback controller

In this paper, we aim at designing a robust controller that could effectively reject disturbance, and the H_∞ performance of the closed-loop system is defined as [20]

$$\left\| G_{cl(p)} \right\|_\infty := \sup_{p \in \Phi_p} \sup_{d \in L_2, \|d\|_2 \neq 0} \frac{\|y\|_2}{\|d\|_2}, \tag{8}$$

where $\Phi_p \in [5\text{psi}, 25\text{psi}]$ is range of the input pressure. It is well known that the H_∞ performance requirement above can be converted to a linear matrix inequality (LMI). Given

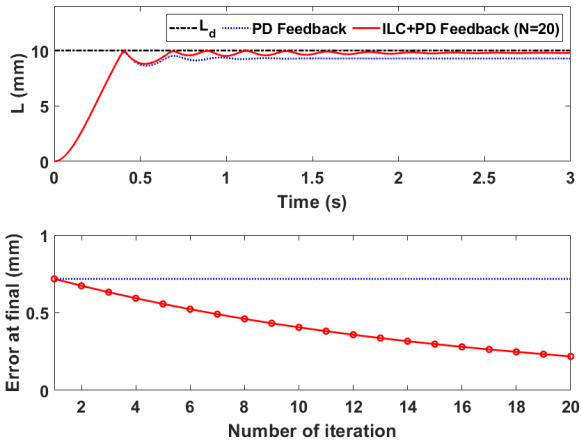

(a) Elongation motion L tracking results

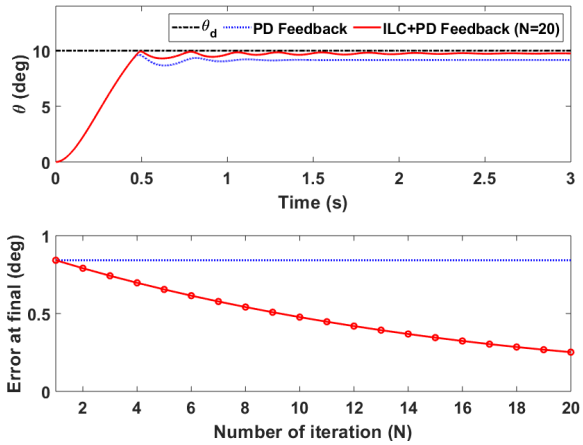

(b) Bending motion θ tracking results

Fig. 7: Simulations of closed-loop system with optimized PD and ILC+PD controllers with a step input

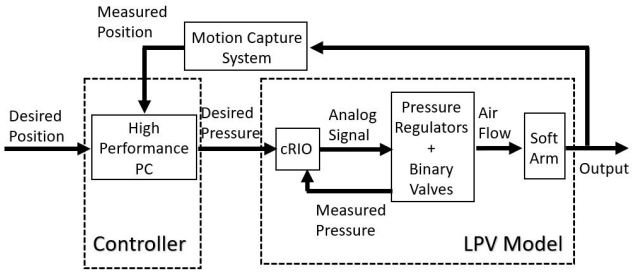

Fig. 8: Hardware diagram for soft arm control system

$\gamma > 0$, the feedback control design with $\left\|G_{cl(p)}\right\|_\infty < \gamma$ can be achieved if there exist matrices $Y \in \mathbb{R}^{1\times 2}$ and $Q = Q^T \in \mathbb{R}^2 > 0$, such that the following LMI holds for all $p \in \Phi_p$ [20]:

$$\begin{bmatrix} A(p)Q + QA^T(p) + B(p)Y + Y^T B^T(p) & * & * \\ CQ & -\gamma & * \\ B^T(p) & 0 & -\gamma \end{bmatrix} < 0 \tag{9}$$

and the corresponding state feedback gain is $K = YQ^{-1}$. It should be noted this will yield a suboptimal controller because we do not minimize the γ, and the reason is to make sure the feedback control gain is not too high. In a motion control system, a high-gain feedback control will make the system very sensitive to measurement noise. In this paper, the resultant gain K is implemented as a PD controller for the system. Figure 5 shows the transfer function between disturbance and output for the closed-loop system with all $p \in \Phi_p$ when $\gamma = 5$, and it can be seen that the closed-loop system can effectively reject disturbance at all frequencies.

B. Motion Control with ILC+state-feedback Controller

Due to the LPV dynamics, a pure state-feedback controller cannot handle the steady-state errors. One possible solution is implementing integration gains to reduce such errors. However, the integration term will amplify the system noise and potentially make the system unstable. Another solution is using the feedforward control and a good choice is the ILC which records errors from previous iterations and generate feedforward inputs to improve the tracking performance.

For a non-linear system, the P-type learning function has been widely used [21]. A continuous-time, P-type learning function can be described as:

$$u^{ff}_{j+1}(t) = u^{ff}_j(t) + k_p e_j(t) \tag{10}$$

where j is the iteration index, k_p is the proportional gain, $u^{ff}(t)$ is the feedforward term and $e(t)$ is the tracking error. The block diagram of the control system is shown in Fig. 6.

V. Simulation

The simulation results of the closed-loop systems are presented in Figs. 7(a) and 7(b). In each simulation, a step reference (desired position or bending angle) is given to the closed-loop system and the steady-state errors from the optimized state-feedback controller which gains from (9) and the combined controller are presented. It can be noted in Fig. 7(a) that given a desired L term, the optimized state-feedback controller reaches a steady state without an overshoot in the elongation motion. However, a residual error of 1 mm is observed at the end of the simulation. To address this residual error, the ILC controller is introduced to the system and the new controller reduces the elongation error.

In Fig. 7(b), the residual error for bending angle θ exists in the optimized state-feedback controller as well and adding the ILC to the system is able to reduce the steady-state errors. In both simulations, the optimized state-feedback gains are relatively large which makes the initial tracking error so small that limited improvement can be achieved by ILC.

VI. Experiments and Results

To validate the performance of both the PD and ILC+PD controllers, the same experimental platform was used to execute the control system presented in Fig. 8. The high performance PC and the motion capture system were connected to the same robot operating system (ROS) server using Ethernet cable to minimize the communication delay. Three markers were placed on the top and bottom of the segment and their positions were tracked and published to the ROS server via motion capture system. The PC subscribed the

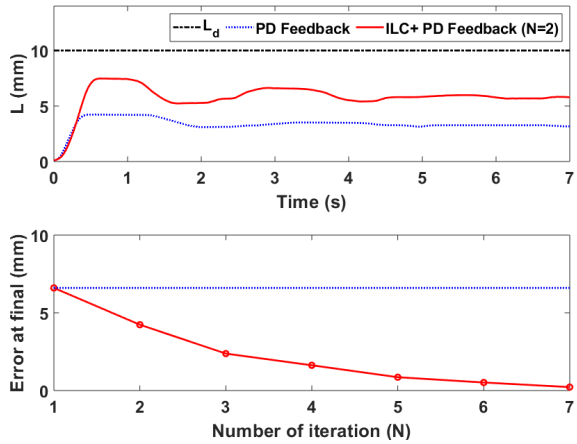

(a) Elongation motion L tracking results

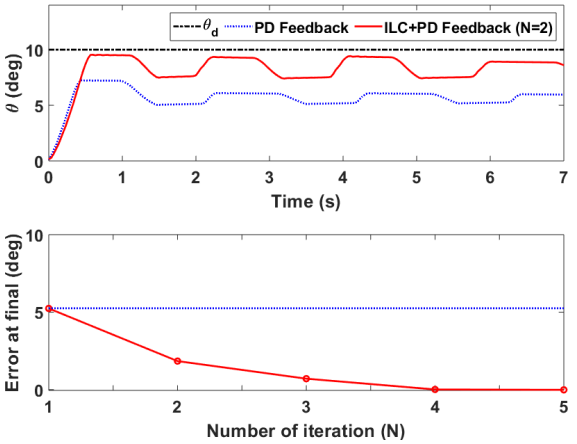

(b) Bending motion θ tracking results

Fig. 9: Experimental results with PD and ILC+PD controllers

markers data at 100 Hz through the server and calculated the desired pressure based on the desired position. Then, the PC sent the calculation results to the NI cRIO using serial communication. The cRIO read and tracked the desired pressure by opening and closing the corresponding valves.

With the state-feedback controller only, the system reached the steady state with a residual error of 6.42 mm, shown in Fig. 9(a). When the ILC was implemented, the segment got closer to the desired posture with an increase of iterations. A similar performance was observed in the bending experiment. Using the same gain sets as the first experiment, the PD controller showed a steady-state error of 5.12 degrees. It was also visible that, in the bending test, the segment periodically oscillated around the steady-state angle. One possible reason was the unknown deflation dynamics. As shown in Fig. 9(b), in the state-feedback experiment, the slopes of the inflation and deflation processes are different. However, in the model, it is assumed that the inflation and deflation follow the same dynamics. This unknown dynamics could introduce modeling uncertainties and hinder the system performance.

In this paper, we only applied the step input to the LPV model and the closed-loop system experiments to present the potential of the proposed model and the model-based control strategies for this soft robotic arm segment. Other typical input, such as sinusoidal signal, will be tested in future experiments. Also, due to the safety concerns, we selected a relatively low input pressure range to identify the model parameters and to validate the proposed closed-loop system performance. A higher range of input pressure would be applied to the system to evaluate this model with larger elongation and bending angles.

VII. CONCLUSION AND FUTURE WORK

In this work, we proposed an LPV model for an elastomer based soft arm and implemented an ILC+state-feedback control algorithm to improve the system tracking performance. The parameters of the LPV model for elongation and bending motion were identified through two sets of experiments. The simulation results of such models showed that the LPV model was able to describe the dynamics of the system. A H_∞ state-feedback control strategy was introduced to the LPV model. Using the LMI method, the optimized gains for the state-feedback controller were identified. However, the residual error existed in the simulation with the optimized state-feedback gains. An ILC with the P-type learning function was implemented into the system with the same PD feedback gains and the steady-state error reduced with the increase of the iterations. The performance of purposed controllers was validated at the custom evaluation platform, and the results matched the mentioned simulations.

Future studies include improving the LPV model performance by identifying the deflation dynamics, applying a wider range of pressure to further validate this model, and combining the model with the motion planning strategy [22] to control the soft robotic arm with multi-segment.

ACKNOWLEDGMENT

We would like to thank Mr. Shatadal Mishra and Mr. Yiwei Wang for their help on the data communication protocol.

REFERENCES

[1] J. Hughes, U. Culha, F. Giardina, F. Guenther, A. Rosendo, and F. Iida, "Soft manipulators and grippers: A review," *Frontiers in Robotics and AI*, vol. 3, p. 69, 2016.

[2] C.-Y. Chu and R. M. Patterson, "Soft robotic devices for hand rehabilitation and assistance: a narrative review," *Journal of NeuroEngineering and Rehabilitation*, vol. 15, no. 1, p. 9, Feb 2018.

[3] I. D. Walker, D. M. Dawson, T. Flash, F. W. Grasso, R. T. Hanlon, B. Hochner, W. M. Kier, C. C. Pagano, C. D. Rahn, and Q. M. Zhang, "Continuum robot arms inspired by cephalopods," in *Unmanned Ground Vehicle Technology VII*, vol. 5804. International Society for Optics and Photonics, 2005, pp. 303–315.

[4] E. W. Hawkes, L. H. Blumenschein, J. D. Greer, and A. M. Okamura, "A soft robot that navigates its environment through growth," *Science Robotics*, vol. 2, no. 8, pp. 1–8, 2017.

[5] Z. Gong, J. Cheng, X. Chen, W. Sun, X. Fang, and K. Hu, "A Bio-inspired Soft Robotic Arm : Kinematic Modeling and Hydrodynamic Experiments," vol. 15, pp. 204–219, 2018.

[6] J. Santoso, E. H. Skorina, M. Luo, R. Yan, and C. D. Onal, "Design and analysis of an origami continuum manipulation module with torsional strength," in *IEEE IROS*, vol. Septe, 2017, pp. 2098–2104.

[7] T. George Thuruthel, Y. Ansari, E. Falotico, and C. Laschi, "Control strategies for soft robotic manipulators: A survey," *Soft Robotics*, vol. 5, no. 2, pp. 149–163, 2018.

[8] A. D. Marchese and D. Rus, "Design, kinematics, and control of a soft spatial fluidic elastomer manipulator," *The International Journal of Robotics Research*, vol. 35, no. 7, pp. 840–869, 2016.

[9] C. Duriez, "Control of elastic soft robots based on real-time finite element method," in *Proc. IEEE ICRA*, 2013, pp. 3982–3987.

[10] N. Farrow and N. Correll, "A soft pneumatic actuator that can sense grasp and touch," in *Proc. IEEE/RSJ IROS*, 2015, pp. 2317–2323.

[11] P. E. Dupont, J. Lock, B. Itkowitz, and E. Butler, "Design and control of concentric-tube robots," *IEEE Transactions on Robotics*, vol. 26, no. 2, pp. 209–225, 2010.

[12] Y. Guo, R. Kang, L. Chen, and J. Dai, "Dynamic modeling for a continuum robot with compliant structure," in *Proc. ASME IDETC/CIE*, 2015, pp. V05AT08A013–V05AT08A013.

[13] J. S. Shamma, "Analysis and design of gain scheduled control systems," Ph.D. dissertation, Massachusetts Institute of Technology, 1988.

[14] M. Van Damme, B. Vanderborght, B. Verrelst, R. Van Ham, F. Daerden, and D. Lefeber, "Proxy-based sliding mode control of a planar pneumatic manipulator," *The International Journal of Robotics Research*, vol. 28, no. 2, pp. 266–284, 2009.

[15] C. M. Best, M. T. Gillespie, P. Hyatt, L. Rupert, V. Sherrod, and M. D. Killpack, "A new soft robot control method: Using model predictive control for a pneumatically actuated humanoid," *IEEE Robotics & Automation Magazine*, vol. 23, no. 3, pp. 75–84, 2016.

[16] D. A. Bristow, M. Tharayil, and A. G. Alleyne, "A survey of iterative learning control," *IEEE Control Systems*, vol. 26, no. 3, pp. 96–114, 2006.

[17] P. H. Nguyen, C. Sparks, S. G. Nuthi, N. M. Vale, and P. Polygerinos, "Soft Poly-Limbs: Toward a New Paradigm of Mobile Manipulation for Daily Living Tasks," *Soft Robotics*, vol. 00, no. 00, p. soro.2018.0065, 2018, (accepted).

[18] P. H. Nguyen, S. Sridar, W. Zhang, and P. Polygerinos, "Design and control of a 3-chambered fiber reinforced soft actuator with off-the-shelf stretch sensors," *International Journal of Intelligent Robotics and Applications*, vol. 1, no. 3, pp. 342–351, 2017.

[19] R. Kang, D. T. Branson, T. Zheng, E. Guglielmino, and D. G. Caldwell, "Design, modeling and control of a pneumatically actuated manipulator inspired by biological continuum structures," *Bioinspiration & biomimetics*, vol. 8, no. 3, p. 036008, 2013.

[20] G. Becker and A. Packard, "Robust performance of linear parametrically varying systems using parametrically-dependent linear feedback," *Systems & Control Letters*, vol. 23, no. 3, pp. 205–215, 1994.

[21] K. L. Moore, *Iterative learning control for deterministic systems*. Springer Science & Business Media, 2012.

[22] W. Zhang and P. Polygerinos, "Distributed planning of multi-segment soft robotic arms," in *2018 Annual American Control Conference (ACC)*. IEEE, 2018, pp. 2096–2101.